



Precessional pacing of tropical ocean carbon export during the Late Cretaceous

Ji-Eun Kim¹, Thomas Westerhold², Laia Alegret³, Anna Joy Drury⁴, Ursula Röhl², and Elizabeth M. Griffith¹

¹School of Earth Sciences, The Ohio State University, Columbus, OH 43210, USA

²Center for Marine Environmental Sciences (MARUM), University of Bremen, 28359 Bremen, Germany

³Department of Earth Sciences, University of Zaragoza, 50009 Zaragoza, Spain

⁴Department of Earth Sciences, University College London, London, WC1E 6BT, UK

Correspondence: Elizabeth M. Griffith (griffith.906@osu.edu) and Thomas Westerhold (twesterhold@marum.de)

Received: 6 May 2022 – Discussion started: 19 May 2022

Revised: 2 November 2022 – Accepted: 5 November 2022 – Published: 16 December 2022

Abstract. The marine biological carbon pump, which exports organic carbon out of the surface ocean, plays an essential role in sequestering carbon from the atmosphere, thus impacting climate and affecting marine ecosystems. Orbital variations in solar insolation modulate these processes, but their influence on the tropical Pacific during the Late Cretaceous is unknown. Here we present a high-resolution composite record of elemental barium from deep-sea sediments as a proxy for organic carbon export out of the surface oceans (i.e., export production) from Shatsky Rise in the tropical Pacific. Variations in export production in the Pacific during the Maastrichtian, from 71.5 to 66 million years ago, were dominated by precession and less so by eccentricity modulation or obliquity, confirming that tropical surface-ocean carbon dynamics were influenced by seasonal insolation in the tropics during this greenhouse period. We suggest that precession paced primary production in the tropical Pacific and recycling in the euphotic zone by changing water column stratification, upwelling intensity, and continental nutrient fluxes. Benthic foraminiferal accumulation rates covaried with export production, providing evidence for benthic–pelagic coupling of the marine biological carbon pump across these high-frequency changes in a cool greenhouse planet.

On timescales of 10 000 to 1 million years, variations in Earth's climate are paced by orbital (Milankovitch) cycles of eccentricity, obliquity, and precession (e.g., 405, 100, 41, and 23–18 kyr) because they alter solar insolation and its distribution on Earth (Laskar et al., 2004, 2011). Orbital-scale climate change is well studied for the Cenozoic Era (e.g., Zachos et al., 2001; Westerhold et al., 2020), but there is limited understanding for earlier times prior to 66 million years. After peak hot greenhouse conditions of the Cretaceous during the Cenomanian about 100 million years ago (e.g., Forster et al., 2007; Huber et al., 2018), progressive global cooling ensued and continued until the end of the Cretaceous (Jenkyns et al., 1994; Friedrich et al., 2012; Voigt et al., 2012). Cool and warm periods were overlaid on the long-term climatic cooling, e.g., the early Maastrichtian cooling pulse (Haynes et al., 2020) and the warm mid-Maastrichtian event (Frank et al., 2005). Extinction of the globally distributed inoceramid bivalves also occurred following a peak in their abundance (e.g., MacLeod and Huber, 1996; Dameron et al., 2017). However, our understanding of the relationship between environmental and biotic change during this time is limited, in part due to the lack of records of key drivers of variability in the ocean–carbon–climate system at orbital timescales in key regions like the tropical Pacific.

Many lines of evidence including climate modeling studies suggest that low- and mid-latitude processes in the climate system respond in nonlinear ways to insolation forcing (e.g., Short et al., 1991; Crowley et al., 1992; Laepple and Lohmann, 2009; Zeebe et al., 2017). In the low-latitudes, eccentricity-modulated precession is expected to dominate

1 Introduction

High-resolution marine sedimentary records are important for shedding new light on critical aspects of Earth's climate and feedbacks in the ocean–atmosphere–biosphere system.

carbon cycle dynamics (Herbert et al., 1999; MacLeod et al., 2001). A key feedback driving these dynamics seems to relate to the global redistribution of moisture and energy by the hydrological cycle (e.g., Trenberth et al., 2000). Proxy records that provide evidence of carbon cycle dynamics, such as marine carbon isotope records ($\delta^{13}\text{C}$), show dominant variability in the eccentricity (rather than precession) band. This effect could be due to the long residence time of carbon in Earth's exogenic system, which filters out higher-resolution fluctuations (e.g., Pälike et al., 2006) or is related to orbitally paced phytoplankton evolution (Beaufort et al., 2022). Nonetheless, during the Late Cretaceous several records outside the tropical Pacific show precession-scale changes in sedimentology and bulk carbonate and foraminiferal carbon isotopes (Herbert et al., 1999; MacLeod et al., 2001; Batenburg et al., 2012, 2014; Barnet et al., 2018, 2019). Whether or not the tropical Pacific carbon cycle, which plays an important role in climate regulation as the largest ocean basin with high burial of pelagic biogenic sediment due to equatorial upwelling, was paced by precession is not clear. The resolution of existing records is insufficient to resolve precessional cycles (Jung et al., 2012, 2013; Voigt et al., 2012; Dameron et al., 2017). Without sufficient sampling resolution of existing records, high-frequency variability in the Earth system could potentially bias conclusions based on unrepresentative or less resolved records (e.g., Herbert et al., 1999).

Here we present an astronomically tuned, high-resolution record of open-ocean organic carbon export, the organic carbon flux out of the surface of the ocean or export production, in the tropical Pacific during the Maastrichtian from 71.5 to 66 million years ago (Fig. 1). Export production is a key organic carbon flux within the marine biological carbon pump which sequesters carbon from the atmosphere to the deep ocean through biologically mediated processes. We use a new composite X-ray fluorescence (XRF) scanning barium (Ba) record as a proxy for export production by comparing it to pelagic marine barite extracted from discrete samples and excess- or bio-Ba measurements on the same samples from the same cores. Accumulation of pelagic marine barite and excess Ba in deep-sea sediments have been shown to correlate with organic carbon flux out of the photic zone (Paytan et al., 1996; Eagle et al., 2003), making these good proxies for export production where there is low terrigenous input and sediment is not sulfate-reducing. We also reconstruct benthic foraminiferal assemblages and accumulation rates over two windows of time to test the relationship between organic carbon export from the surface ocean represented by the Ba records and organic carbon reaching the seafloor (i.e., the sequestration flux), represented by the benthic foraminiferal records. These new records allow us to better characterize the marine biological pump at this time and show that precession, rather than eccentricity or obliquity, was the dominant orbital cycle that paced ocean export production, thereby in-

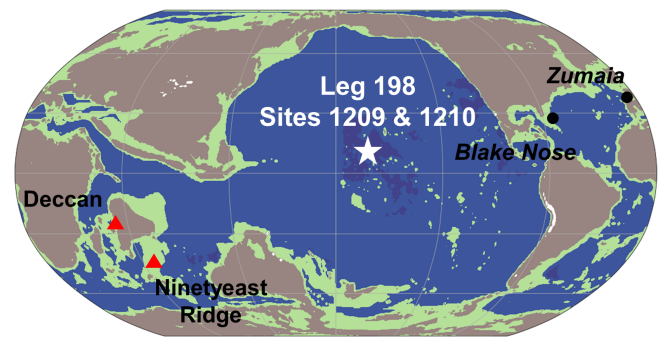


Figure 1. Location of ODP Leg 198 Sites 1209 and 1210 at Shatsky Rise at 69 Ma (star) in the tropical Pacific (Scotese and Wright, 2018). Deccan and Ninetyeast Ridge are shown as red triangles. Location of Zumaia (Batenburg et al., 2012, 2014) and Blake Nose (MacLeod et al., 2001) records are shown as black circles. Shading indicates land above 0 m (brown); land above 6 km (white); and ocean settings with water depths greater than 4 km (dark blue), between 4 km and 120 m (blue), and above 120 m (green).

fluencing the marine carbon cycle in the tropics during the Maastrichtian cool greenhouse period.

2 Materials and methods

2.1 Study site

Shatsky Rise formed about 145 million years ago in the Pacific (Larson et al., 1992; Sager et al., 1999), providing an archive of Cretaceous sediments in the tropics thought to have been above the carbonate compensation depth (CCD) between 1500 and 2000 m throughout their deposition (Sager et al., 1999). The current locations of Ocean Drilling Program (ODP) Leg 198 Sites 1209 and 1210 are $32^{\circ}39.1081' \text{ N}$, $158^{\circ}30.3564' \text{ E}$ (2387 m below sea level) and $32^{\circ}13.420' \text{ N}$, $158^{\circ}15.5623' \text{ E}$ (2573 m below sea level), respectively (Bralower et al., 2002). Shatsky Rise drifted northward on the Pacific plate to its present location (Larson et al., 1992; Dameron et al., 2017). During the Late Cretaceous, Shatsky Rise was approximately 10° N of the Equator (Fig. 1; Larson et al., 1992; Dameron et al., 2017) in a region of relatively high productivity due to upwelling caused by the divergence of the North Equatorial Counter Current and the North Equatorial Current. Previous studies on the Maastrichtian at Sites 1209 and 1210 identified the inoceanic acme and extinction, changes in ocean circulation, carbonate dissolution, and episodes of higher productivity prior to the end-Cretaceous extinction event 66.0 million years ago (Bralower et al., 2002; Frank et al., 2005; Alegret and Thomas, 2009; Jung et al., 2012, 2013; Renne et al., 2013; Dameron et al., 2017). However, prior age models (Fig. S1 in the Supplement) and data resolution were incomplete and insufficient to identify precessional cycles in these open-ocean tropical Pacific sedimentary records.

2.2 Samples

This study used deep-sea marine sediment samples from ODP Leg 198 Sites 1209 and 1210 on Shatsky Rise, north-western Pacific, during the Maastrichtian (from 71.5 to 66 million years ago) to create a continuous composite record. Samples consisted primarily of very pale orange to white nannofossil ooze, mostly > 96 wt % (weight percent) CaCO₃ and discontinuous chert nodules likely formed by remobilized biogenic silica (Bralower et al., 2002). Bulk carbonate $\delta^{18}\text{O}$ and $\delta^{13}\text{C}$ were measured in 1394 samples from both Sites 1209 (1096) and 1210 (298) about every 5 cm. Discrete samples from 5 intervals that consist of 51 samples in total included Samples 1209C-16H-1 (114 to 145 cm), 1209C-21H-1 (67 to 118 cm), 1209C-22H-2 (133 cm) to 1209C-22H-3 (31 cm), 1209B-29H-1 (87 cm) to 1209B-29H-2 (20 cm), and 1210B-25H-4 (43 to 80 cm). Samples were taken every 5 cm or so in the core and weigh between 13 and 22 g (approximately 20 cm³). Additional samples for benthic foraminifera were taken from over two of the five intervals that have barite data.

2.3 Bulk stable carbon and oxygen isotopes

Bulk carbonate $\delta^{13}\text{C}$ and $\delta^{18}\text{O}$ analyses (Datasets S1–S3 in the Supplement) on 1394 freeze-dried and pulverized sediment samples from Sites 1209 (1096) and 1210 (298) were performed at MARUM, University of Bremen. The bulk stable carbon and oxygen isotope data are reported relative to the Vienna Pee Dee Belemnite (VPDB) international standard, determined via adjustment to calibrated in-house standards and NBS-19. Bulk carbonate analyses were carried out on a Finnigan MAT 251 mass spectrometer equipped with an automated carbonate preparation line (Kiel III). Carbonate was reacted with orthophosphoric acid at 75 °C. Analytical precision based on replicate analyses of an in-house standard (Solnhofen Limestone) is 0.04 ‰ (1 σ) for $\delta^{13}\text{C}$ and 0.07 ‰ (1 σ) for $\delta^{18}\text{O}$.

2.4 Scanning XRF Ba

Non-destructive X-ray fluorescence (XRF) data were collected every 2 cm down-core using an XRF core scanner (Avaatech serial no. 17) from the XRF core scanning facility at the International Ocean Discovery Program's (IODP) Gulf Coast Repository at Texas A&M University (College Station, USA) in March 2017 for Sites 1209 and 1210 (Datasets S4–S6). Data were collected over a 1.2 cm² area with a down-core slit size of 10 mm using generator settings of 50 kV and a current of 0.75 mA, ideally for detecting Ba, and a sampling time of 12 s in each run directly at the split core surface of the archive half. The split core surface was covered with a 4 μm thin SPEX CertiPrep Ultralene foil to avoid contamination of the XRF detector prism and desiccation of the cores. The data were acquired with a SiriusSD 65 mm² silicon drift detector model 878-0616B – SGX Sensortech with

133 eV X-ray resolution at 5.9 keV and 3 kcps, the Canberra digital spectrum analyzer DAS 1000, and an Oxford Instruments 50 W Neptune X-ray tube with a rhodium (Rh) target. Raw data spectra were processed using the analysis of X-ray spectra by the iterative least square software (bAxil) package from Canberra Eurisys. The scanning XRF Ba was used as a qualitative record of changes in biogenic barium flux at this open-ocean setting after assessing minimal difference between XRF Ba and XRF Ba normalized to “total area” (the sum of all counts for all elements processed from the 50 kV run data) (XRF Ba / total area), as shown in Fig. S2, to confirm that there is little to no volume effect on scanning XRF Ba trends. Additionally, the XRF Sr / total area ratio (Fig. S3) is shown.

2.5 Composite record

The scanning XRF Ba elemental intensities were used to correlate Maastrichtian cores from ODP Leg 198 Holes 1209A, 1209B, and 1209C as well as Holes 1210A and 1210B to establish new composite records for Site 1209 and 1210 (Figs. S4–S6). Additionally, all core intervals outside the composite were mapped to the composite to place data from those intervals on the new splice. All relevant tables for composite constructions are given in Datasets S7–S9 for Site 1209 and Datasets S10–S12 for Site 1210. To form a complete Maastrichtian succession both sites had to be combined to cover gaps and avoid drilling disturbed intervals. Correlation tie points using XRF Ba elemental intensities (Fig. S6) are given in Dataset S13.

2.6 Barite accumulation rate (BAR)

Barite separation was done on all 51 discrete sediment samples across 5 intervals (Dataset S14). The barite separation method, which dissolves carbonates, organic matter, Fe–Mn oxyhydroxides, silicates, and fluorides to obtain a purified barite residue, was modified from Paytan et al. (1996) as outlined in Table S1 in the Supplement. Specifically, acetic acid was used to slowly (but completely) dissolve carbonates because the samples had such high carbonate content (> 96 wt %). Sample ashing in a furnace to remove refractory organic material was done after the scanning electron microscope (SEM) observation due to the low weight of the residue (and low organic material content). Previous work (Eagle et al., 2003) showed that the barite separation method of Paytan et al. (1996) resulted in less than 5 % loss of original barite when followed accordingly. Each sample residue was then imaged using a Hitachi Benchtop SEM TM3030 at Kent State University to determine the average percentage of barite (i.e., purity) by taking images of five random spots (Fig. S7). The purity was multiplied by the dry weight of the residue and divided by the total dry bulk sample weight to determine the pelagic marine barite weight percent.

Barite accumulation rate (BAR) was then calculated by multiplying the pelagic marine barite weight percent by the mass accumulation rate (MAR). This corrects any bias using weight percent data that could result from varying linear sedimentation rate (LSR) or changes in dry bulk density (DBD). To determine the MAR, the linear sedimentation rate (LSR) was multiplied by dry bulk density (DBD) from Bralower et al. (2002). Dry density in each core section was used where available, such as for core section 198-1210B-25H-4. When there was no dry density measured for the specific core section, the nearby dry density average was taken (1209B-27H-6 and 1209B-31H-1 DBD were used for 1209B-29H-1 and 1209B-29H-2 and 1209C-21H-1), or the nearest DBD was adopted (1209A-26H-4 was used for 1209C-16H; 1209B-31H-6 DBD was used for 1209C-22H-2 and 1209C-22H-3).

2.7 Excess-Ba (bio-Ba) accumulation rate (excess-BaAR)

Bulk digestion of aliquots of the same discrete bulk samples used for barite separation above was done to determine excess-Ba (i.e., biogenic Ba) content from measurements of Ba and Al (Dataset S15). A modified bulk digestion method from Scudder et al. (2014) was used as outlined in Table S2, and the resulting solution was measured using a Perkin Elmer 3000DV inductively coupled plasma optical emission spectrophotometer (ICP-OES) in the Trace Element Research Lab at The Ohio State University. Table S3 shows the wavelength for each element analyzed and relative standard deviation (2RSD), determined from replicate analyses of the medium standard solution ($n = 7$). Measurements were 4 % (2RSD) for Ba. Other elements (Ca, Fe, Al, Ti, Mn, Mg, Sr, and K) had 2RSD ranging from 2 % to 3 %, but Si had 2RSD of 16 %.

Excess Ba was calculated using an equation (Sect. S1 in the Supplement) from Dymond et al. (1992) which corrects for any contribution of non-biogenic Ba. For this study, a terrigenous Ba/Al ratio ($Ba/Al_{\text{terrigenous}}$) of 0.0037 was used (Reitz et al., 2004). Additional corrections for Ba associated with authigenic components and Fe-smectite using measurements of Mn and Fe (Olivarez Lyle and Lyle, 2006) were not needed as these corrections resulted in differences of 6 % or less (on average 2 % difference; see Sect. S1). Excess-Ba accumulation rate (excess-BaAR) was then calculated by multiplying the excess Ba (ppm) by the MAR as determined above.

2.8 Benthic foraminiferal data

For quantitative studies of benthic foraminifera (Dataset S16) 16 selected samples were taken from the cores of Site 1209 spanning several cycles observed in scanning XRF Ba data. Samples of 10 to 15 cm³ were taken at the Gulf Core Repository (GRC), then oven-dried at < 50 °C overnight and washed using tap water over a 63 µm sieve to extract the

sand-sized fraction at MARUM Bremen. Wet-sieved samples were oven-dried at < 50 °C overnight and weighed to determine coarse fraction weight %. Benthic foraminiferal quantitative analysis was carried out at University of Zaragoza based on representative splits of approximately 300 specimens larger than 63 µm. The percentages of individual taxa, species with agglutinated tests, and the superfamily Buliminacea were calculated (Dataset S16). The benthic foraminiferal accumulation rates (BFARs) were calculated as a qualitative proxy for delivery of organic matter to the seafloor (Jorissen et al., 2007), using the number of benthic foraminifera per gram of sediment > 63 µm, the weight % of the sample > 63 µm, the linear sedimentation rate and the sediment density. BFARs are expressed as the number of benthic foraminifera (nr) accumulated per square centimeter and per 1000 years.

3 Astrochronology and cyclostratigraphy

Using the shipboard biostratigraphic datums (Fig. S1) and time series analysis we find that the composite bulk $\delta^{13}\text{C}$ record of Shatsky Rise ODP Sites 1209 and 1210 reveals a strong imprint of the 405 kyr long eccentricity cycle (Fig. 2). For an initial 405 kyr age model the composite bulk $\delta^{13}\text{C}$ record was filtered for the 405 kyr cycle in the depth domain (5 m bandpass filter using 0.2 ± 0.06). Then the 13 identified 405 kyr cycles were correlated to the Laskar et al. (2004) and Laskar (2020) cosine function with correlating maxima in the $\delta^{13}\text{C}$ filter to minima in the cosine function (Fig. 3). This phase relationship follows the findings in the Zumaia section from the Basque Country in northern Spain (Batenburg et al., 2012) and provides a basic 405 kyr stratigraphy without introducing short eccentricity, obliquity, or precession component features into the records. The age tie points for the 405 kyr age model are in Table S4. To test the completeness of the Shatsky Rise record, we used the tie points of Batenburg et al. (2012) updated for the Laskar cosine function for the Zumaia succession and plotted bulk $\delta^{13}\text{C}$ records (Fig. S8, Table S5). The match of both records is remarkable, suggesting that both Zumaia and Shatsky Rise recorded global carbon cycle variations.

The power ratio method used here can be subjective, and thus we tested the record with the more complex statistical tool of the correlation coefficient (COCO) and evolutionary correlation coefficient (eCOCO) embedded in the *Acycle* software package (Li et al., 2019). Using *Acycle* the results are indeed basically the same as those done by the more simplistic power ratio method showing a most likely sedimentation rate at $\sim 1.3 \text{ cm kyr}^{-1}$ (Fig. S9). The eCOCO method reveals a minor discrepancy at $\sim 285 \text{ m}$, which corresponds to the depth between 405 kyr cycles labeled Maa5 and Maa6 in Fig. 3 (and Fig. S8). If we assume that there is one more 405 kyr cycle in this interval, the carbon isotope minimum at 68.3 Ma would not match the Zumaia record any-

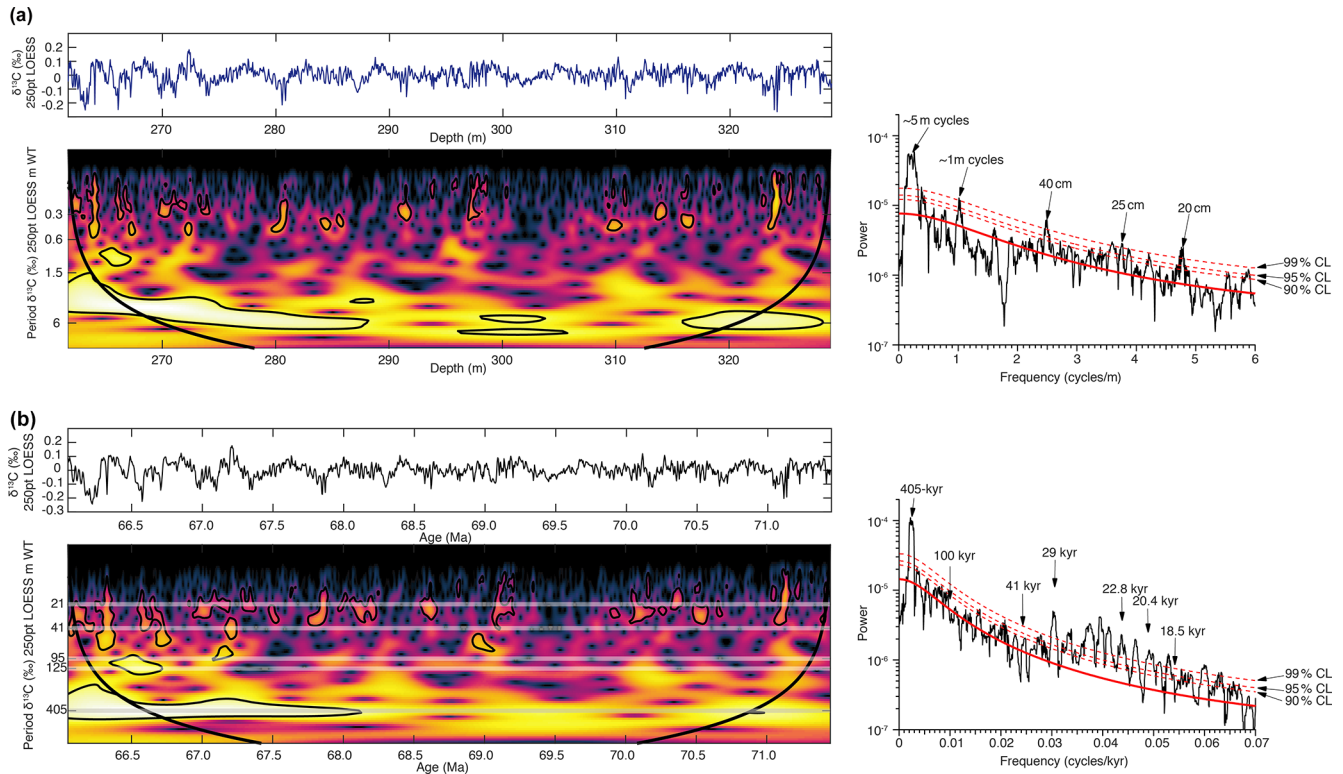


Figure 2. (a) Bulk carbonate $\delta^{13}\text{C}$ by depth (m) shown with 250-point LOESS smoothing and wavelet analysis (Torrence and Compo, 1998; Grinsted et al., 2004) and the multi-taper method (MTM) shown for spectral analysis. (b) $\delta^{13}\text{C}$ by age (Ma) shown with 250-point LOESS smoothing and wavelet analysis and MTM shown for spectral analysis. CL indicates confidence level. Note age is increasing from the left to right.

more. It should be pointed out here that the drill cores used are affected by coring disturbance to some extent, particularly when chert layers were encountered. For the composite record from Shatsky Rise, we tried to avoid these intervals whenever possible. Some disturbance and therefore misinterpretation of changes in cycle thickness can occur using an automated analysis routine that assumes constant sedimentation rates. We thus use the 405 kyr astronomically tuned age model presented here to reconstruct open-ocean organic carbon export at high resolution in the tropical Pacific during the Maastrichtian from 71.5 to 66 Ma.

4 Proxy results and discussion

4.1 Export production proxies

Pelagic marine barite weight percent (wt %) and excess Ba determined on the same samples between 71.5 and 66 Ma are positively correlated (Fig. 4), confirming that excess Ba represents the biogenic or pelagic marine barite formed in the water column within microenvironments of decaying organic matter (Paytan et al., 1996). For the same or neighboring samples (within 1 cm), X-ray fluorescence (XRF) Ba also has a strong positive correlation with both pelagic ma-

rine barite and excess Ba. After calculating and comparing accumulation rates of barite (BAR) and excess Ba (excess-BaAR) to scanning XRF Ba, the strong positive correlation remains (Fig. S10). This confirms that all barium records represent changes in export production in these sediments.

The equivalent barite accumulation from excess-barite measurements, however, is higher than that determined from extracting barite. Either non-barite (i.e., non-biogenic) Ba phases are included in the excess-Ba data biasing the data (Murray et al., 2000; Eagle et al., 2003; Gonnee and Paytan, 2006), or BAR is underestimating barite accumulation due to the mechanical loss of barite or its dissolution during sample processing, which is possible for samples with low barite weight percent (Eagle et al., 2003). Such offsets between proxies are a concern when trying to precisely quantify variations in proxy measurements in terms of export production. Nonetheless, offsets are less of a concern when looking at one site over time and comparing trends qualitatively to determine relative changes in export production, such as for this study. Therefore, we conclude that scanning XRF Ba is a valid proxy to reconstruct export production at high resolution in the open-ocean tropical Pacific at Sites 1209 and 1210 during the Maastrichtian.

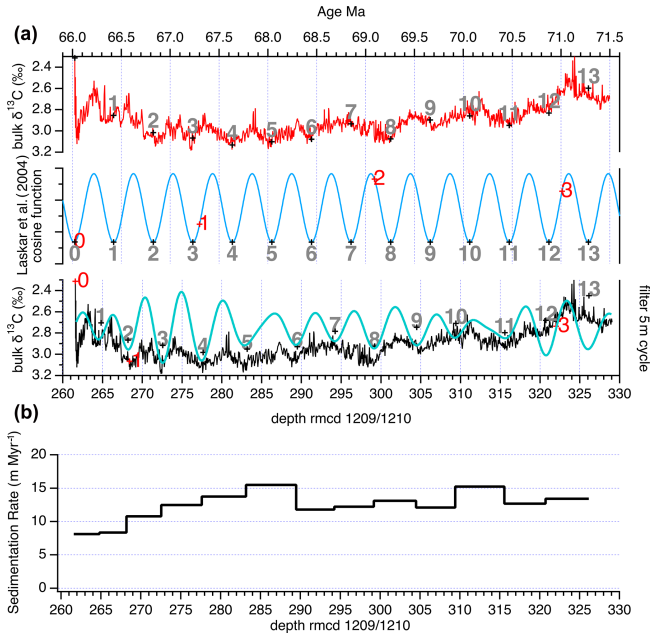


Figure 3. (a) Basic 405 kyr age model was first made by assigning Shatsky Rise Sites 1209 and 1210 composite bulk $\delta^{13}\text{C}$ to known tie points (red numbers). Then, a 5 m filter (bandpass 0.2 ± 0.06) of bulk $\delta^{13}\text{C}$ composite was modeled to know the cosine function (cyan line). This cosine function was correlated to the La2004 cosine function (Laskar et al., 2004; blue line) minima for tuning the depth to the stable 405 kyr cycle for an age. New age is tie points in Table S4. (b) Sedimentation rate in meters per million years (m Myr^{-1}) of composite depth (rmcd).

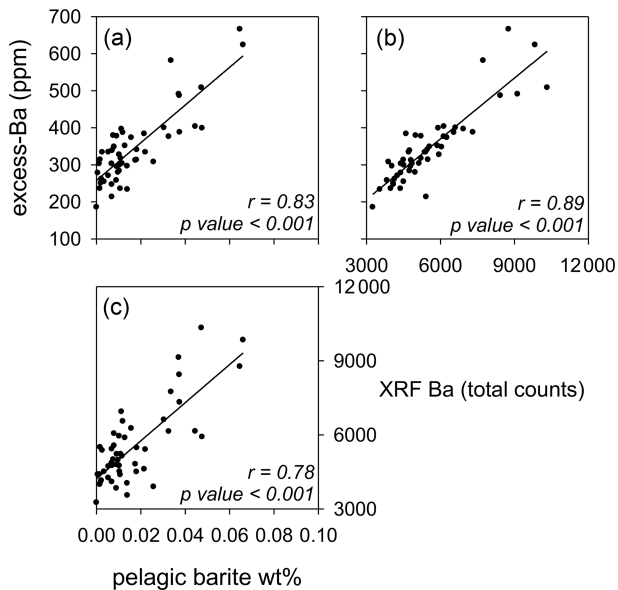


Figure 4. Pelagic marine barite weight percent (wt %), (a, b) excess Ba (ppm), and (c) XRF Ba (total counts) compared to each other. All correlations between barite-related proxies are significant ($p < 0.001$).

4.2 Orbital cyclicity in the tropical Pacific biological pump

We observe orbital cyclicity in the continuous composite records of scanning XRF Ba and bulk carbonate $\delta^{13}\text{C}$ and $\delta^{18}\text{O}$ from Sites 1209 and 1210 (Figs. 2, 5, S11, and S12). While the 405 kyr long eccentricity used to constrain the age model dominates bulk carbonate $\delta^{13}\text{C}$, it is less dominant in bulk carbonate $\delta^{18}\text{O}$ and least dominant in the scanning XRF Ba. This suggests that bulk carbonate $\delta^{13}\text{C}$ is primarily responding to factors other than temperature or salinity and organic C export, which impact the bulk carbonate $\delta^{18}\text{O}$ and scanning XRF Ba, respectively. Because the bulk carbonate $\delta^{13}\text{C}$ values closely resemble the lower-resolution surface planktic foraminiferal $\delta^{13}\text{C}$ record of *Rugoglobigerina rugosa* (Fig. S3) from the same sites reported by Jung et al. (2013), it is possible that it reflects surface conditions potentially related to local surface productivity. However additional high-resolution work is needed to confirm this initial observation. The 100 kyr short-eccentricity cycle is weak in all three records, and obliquity is not present in any of the records. Precession is observed in all records but is strongest in XRF Ba, demonstrating that precession, not the modulating eccentricity cycle, played the major role in pacing organic C export or export production in the tropical Pacific during the Maastrichtian.

The variations in scanning XRF Ba throughout the composite record are interpreted as variations in export production and provide robust evidence for a tropical Pacific Ocean dominated by low-latitude (precessional) climate variations which responded strongly to precession even when the amplitude was low (e.g., during 100 kyr eccentricity minima). When combined with existing records from the Atlantic during the Late Cretaceous (e.g., Herbert and D'Hondt, 1990; Herbert et al., 1999; MacLeod et al., 2001; Batenburg et al., 2012, 2014), a significant response of the Earth system due to the orbital forcing of precession is clear (Herbert et al., 1999; Clement et al., 2004).

The BAR and excess-BaAR records show export production increased by a factor of 2 to 4 within a single precessional cycle, in step with changes in scanning XRF Ba (Figs. 6 and S13). These large changes in the flux of organic matter falling through the water column can be caused by changes in surface production, transport efficiency, or both (Murray et al., 1996; Griffith et al., 2021). These data also suggest that these sites had generally low rates of new production ($< 2.2 \text{ gC cm}^{-2} \text{ yr}^{-1}$ using Dymond et al., 1992; see Sect. S2) or that a very small fraction of the surface production was exported to depth (i.e., low transfer efficiency).

During these same precessional cycles, the barite-related proxies are in phase with the amount of exported organic matter that reaches the seafloor (i.e., sequestration flux), reconstructed using benthic foraminifera accumulation rates (BFARs; e.g., Alegret et al., 2012, 2020; Griffith et al., 2021) (Fig. 6). A similar trend is shown in the percentage of

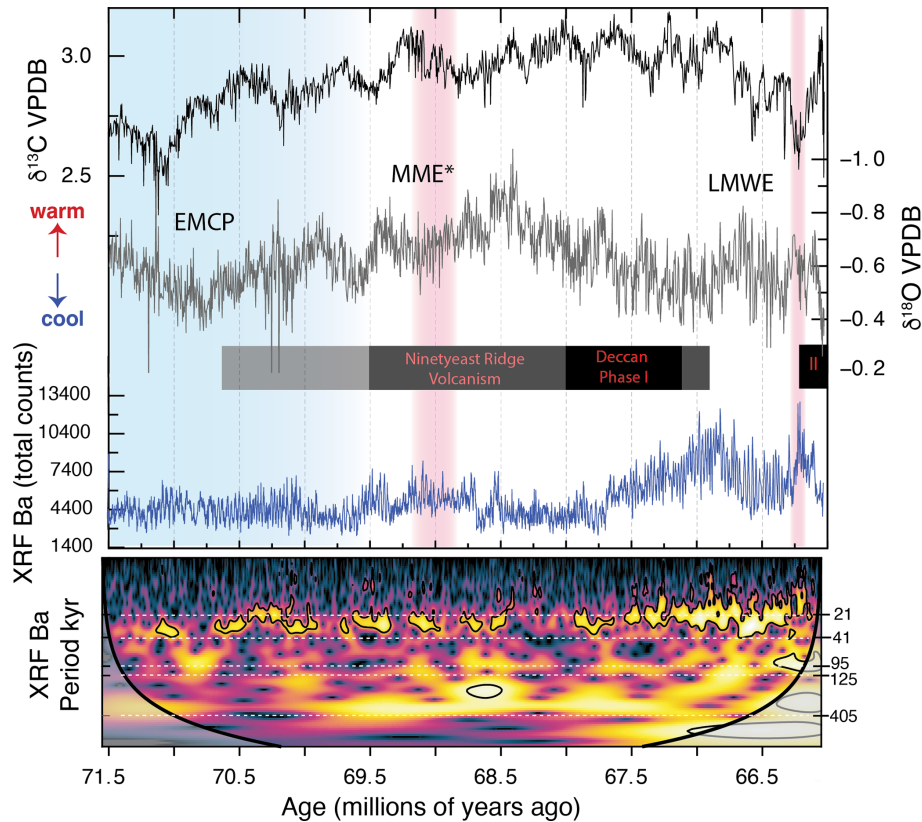


Figure 5. Bulk carbonate $\delta^{13}\text{C}$, $\delta^{18}\text{O}$, scanning XRF Ba, and wavelet analysis (Torrence and Compo, 1998; Grinsted et al., 2004) on non-stationary periodicities for XRF Ba (500 LOESS composite of Sites 1209 and 1210) show signals of precession in scanning XRF Ba which strengthen after Deccan volcanism begins. Brighter colors correspond to higher power within a corresponding frequency period (in thousands of years, kyr). Ninetyeast hotspot volcanism and approximate duration of Deccan volcanism shown, adapted from Keller et al. (2016). EMCP: early Maastrichtian cooling pulse (Haynes et al., 2020); MME*: mid-Maastrichtian event beginning at Chron C31n and lasting ~ 500 kyr (Voigt et al., 2012); LMWE: latest Maastrichtian warming event (Li and Keller, 1998).

the superfamily Buliminacea, which in the absence of low-oxygen conditions is indicative of enhanced food supply to the seafloor (Jorissen et al., 2007; Alegret et al., 2012), and the percentage of the oligotrophic species *Oridorsalis umbonatus* is higher when Ba drops in the intervals of low export productivity (Fig. S14). These results suggest coupling between export production and carbon sequestration (i.e., carbon reaching the seafloor) in the tropical Pacific open ocean during the Maastrichtian. The variability in these short but high-resolution records is similar to that of lower-resolution records (e.g., Frank et al., 2005), suggesting that caution is needed when interpreting lower-resolution records of a highly variable signal, where drivers of variability can be masked in the lower-resolution records.

4.3 Direct response to precession during greenhouse

Carbon export from the surface ocean in the tropical Pacific (evidenced by XRF-Ba content) appears to have changed as a direct response to high-frequency (~ 21 kyr), seasonal, insolation-forced tropical precipitation. This fingerprint of

precession in the deep-sea sedimentary record is most simply explained as the result of variations in surface productivity forced by cyclic variation in water column stratification, upwelling intensity, and continental nutrient fluxes. In the tropical Pacific, where the thermocline depth has a strong influence on ocean primary production (Turk et al., 2001), a ~ 21 kyr precession cycle could have been dominant in the Maastrichtian (Fig. 7). Shoaling of the thermocline would result in increased primary production and carbon export due to enhanced upwelling of nutrients, and this new record suggests such variations could have occurred in response to changes in precession. Previous work suggested a link between past warm climates and a “permanent El Niño” state (Wara et al., 2005; Fedorov et al., 2006) with weak trade winds along the Equator, a deeper thermocline, and a more stratified tropical Pacific preventing upwelling of nutrients, which resulted in reduced primary production and low carbon export. Today this scenario occurs as an irregular periodic variation along with an opposite “La Niña” state in the tropical Pacific, with strong trade winds and more intense upwelling in the eastern tropical Pacific driving increased

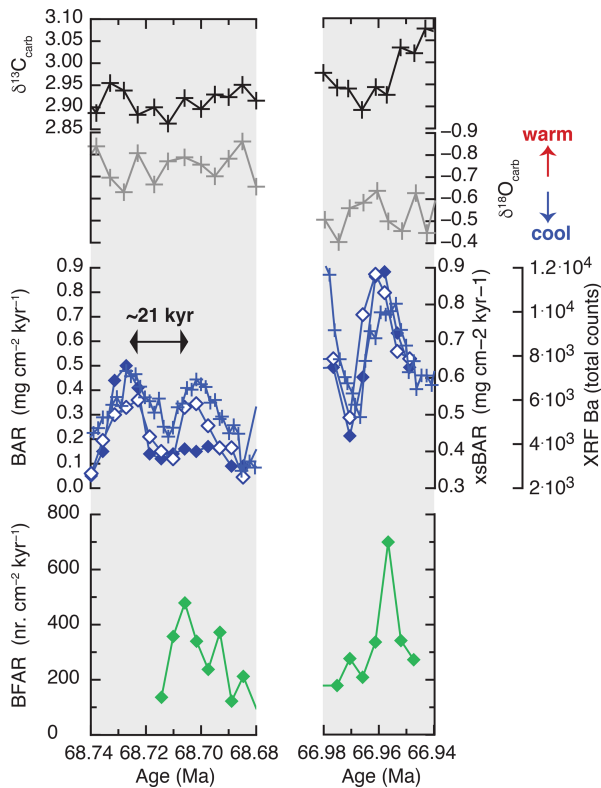


Figure 6. Two discrete sample intervals covering potential cycles of precession (~ 21 kyr) with surface-water-related proxies (bulk $\delta^{13}\text{C}$, $\delta^{18}\text{O}$), organic carbon export proxies (scanning XRF Ba: crosses; excess-BaAR: open diamonds; and BAR: solid diamonds), and proxy for organic carbon arrival at the seafloor (BFAR: green diamonds). A positive correspondence is seen between carbon export from the surface of the oceans (XRF Ba, excess-BaAR, BAR) and organic carbon arrival at the seafloor (BFAR).

productivity on interannual to decadal timescales. Changes in the mean state over longer timescales can be recorded in deep-sea sediment archives (e.g., Pena et al., 2008; Zhang et al., 2021). The large range of variations in our carbon export record in the tropical Pacific (XRF-Ba elemental intensities and benthic foraminiferal accumulation rates) during the Maastrichtian greenhouse argues against the hypothesis of a continual or permanent El Niño-like state. Our record exhibits variations which could reflect changes in the mean climate state. We suggest that this new record adds to the growing body of evidence that suggests robust El Niño–Southern Oscillation (ENSO)-like variability existed in past greenhouse conditions (e.g., Davies et al., 2012), and this ENSO-like variability may be sensitive to orbital forcing, especially the effect of orbital precession in the tropics (e.g., Clement et al., 1999, 2000; Lu et al., 2019). The resulting tropical mean climate state and climate variability forced by precession minima or maxima changing the strength of coupled ocean–atmosphere feedbacks in the tropical Pacific are less clear during the Maastrichtian greenhouse (Fig. 7) and

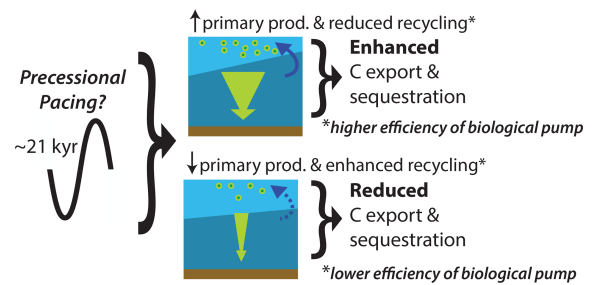


Figure 7. Cycles of enhanced and reduced carbon (C) export and sequestration result from precessional paced variations in primary productivity and recycling in surface waters (i.e., changes in the efficiency of the biological pump). A shallower thermocline (steeper boundary between light- and dark-blue waters) would result in increased primary production and reduced recycling in the surface waters due to changes in water column stratification, continental nutrient fluxes, and upwelling intensity which increases nutrients (solid blue arrow) and enhances C export out of the surface waters (wide green arrow). A deeper thermocline (near horizontal boundary between light- and dark-blue waters) would result in reduced primary production and enhanced recycling in the surface waters due to reduced nutrient availability (dashed blue arrow) and reduces C export out of the surface waters (thin green arrow). This ENSO-like variability could have controlled carbon export in the Maastrichtian.

require focused modeling efforts and new proxy records to test these hypothesized relationships.

Reduced stratification and enhanced upwelling increase primary production and organic carbon export but are expected to induce a greater release of CO_2 to the atmosphere and act as a positive feedback to warming, unless the enhanced biological pump effectively suppresses the increase in CO_2 outgassing due to enhanced upwelling (e.g., Kim et al., 2019). Increased organic carbon export would also increase the corrosivity of deeper waters (e.g., Lyle et al., 1995), although CaCO_3 content in sediments remained high throughout this time at this site ($> 95\%$; Dataset S14). The maxima in corrosion-resistant benthic foraminifera (*N. truempyi*) and percent of agglutinated taxa, however, coincide with Ba maxima, providing further support of increased organic carbon export (Fig. S14).

The high-frequency, precessional pacing of the carbon export in the tropical Pacific persisted throughout the Maastrichtian. This suggests it was a consistent, intrinsic feature of the end-Cretaceous cool greenhouse, despite longer (and larger) scale changes, e.g., early Maastrichtian cooling pulse (EMCP; Haynes et al., 2020), warm mid-Maastrichtian event (MME; MacLeod and Huber, 1996), the early phase of Deccan Traps volcanism (67.5 to 67.1 Ma; Chenet et al., 2007; Keller et al., 2016), or the Latest Maastrichtian Warming Event (LMWE; Li and Keller, 1998; Gilbert et al., 2021). Organic carbon export appears largely decoupled from the abundance and eventual extinction of inoceramid bivalves related to the MME, suggesting that additional drivers (e.g.,

emplacement of large igneous provinces) played an important role in biotic change during this time. An increase in amplitude of the variations in carbon export recorded towards the end of the Cretaceous suggests an amplified sensitivity to orbital forcing when CO₂ was higher during Deccan volcanism, beginning around 67.5 Ma (Chenet et al., 2007). As anthropogenic CO₂ emissions increase today, we need to consider whether or not sensitivity to seasonal insolation in the tropics might increase and dominate changes in the ocean–carbon–climate system in this key region.

Data availability. All data are available at PANGAEA (<https://doi.org/10.1594/PANGAEA.951175>; Kim et al., 2022).

Supplement. The supplement related to this article is available online at: <https://doi.org/10.5194/cp-18-2631-2022-supplement>.

Author contributions. All authors contributed to the ideas expressed in this paper. TW initiated this project, which was further developed by EMG and JEK; TW and UR analyzed XRF and bulk carbonate isotopes; JEK prepared and analyzed barite samples under the guidance of EMG; LA prepared and analyzed the benthic foraminiferal results. TW created the age model and composite record. JEK, EMG, TW, LA, and AJD did the artwork. All authors contributed to data interpretation and manuscript writing.

Competing interests. The contact author has declared that none of the authors has any competing interests.

Disclaimer. Publisher's note: Copernicus Publications remains neutral with regard to jurisdictional claims in published maps and institutional affiliations.

Acknowledgements. Samples were provided by the International Ocean Drilling Program. We thank the staff at the IODP Gulf Coast Core Repository (GCR) for assistance at the Texas A&M University XRF Core Scanner Lab and sampling guidance. We also thank Faizura Ahmad Zulkifli and Anis Hishammudin for assistance in barite separation, Samantha Carter for supervision on the separation process, Julia Sheets and Susan Welch for supervision on SEM sample coating, Anthony Lutton for supervision on ICP measurements, Merida Keatts at Kent State University for supervision on the SEM operation, and Jason Curtis at University of Florida for processing the carbonate weight percent.

Financial support. This research has been supported by the Deutsche Forschungsgemeinschaft (DFG, German Research Foundation), who provided funding to Thomas Westerhold and Ursula Röhl (project no. 320221997), and by grant no. PID2019-105537RB-I00 funded by MCIN/AEI/10.13039/501100011033 and

by “ERDF A way of making Europe” to Laia Alegret. Funding was also provided by the Deutsche Forschungsgemeinschaft (DFG, German Research Foundation) under Germany's Excellence Strategy – EXC-2077 – 390741603. This work was also supported in part by Ohio State Friends of Orton Hall, who provided funding to Ji-Eun Kim, and US National Science Foundation grant no. OCE-1536630 to Elizabeth M. Griffith.

Review statement. This paper was edited by Zhengtang Guo and reviewed by Mingsong Li and one anonymous referee.

References

- Alegret, L. and Thomas, E.: Food supply to the seafloor in the Pacific Ocean after the Cretaceous/Paleogene boundary event, *Mar. Micropaleontol.*, 73, 105–116, <https://doi.org/10.1016/j.marmicro.2009.07.005>, 2009.
- Alegret, L., Thomas, E., and Lohmann, K. C.: End-Cretaceous marine mass extinction not caused by productivity collapse, *P. Natl. Acad. Sci. USA*, 109, 728–732, <https://doi.org/10.1073/pnas.1110601109>, 2012.
- Alegret, L., Arreguín-Rodríguez, G. J., Traviña-Moreno, C. A., and Thomas, E.: Turnover and stability in the deep sea: Benthic foraminifera as tracers of Paleogene global change, *Global Planet. Change*, 196, 103372, <https://doi.org/10.1016/j.gloplacha.2020.103372>, 2020.
- Barnet, J. S., Littler, K., Kroon, D., Leng, M. J., Westerhold, T., Röhl, U., and Zachos, J. C.: A new high-resolution chronology for the Late Maastrichtian warming event: Establishing robust temporal links with the onset of Deccan volcanism, *Geology*, 46, 147–150, 2018.
- Barnet, J. S., Littler, K., Westerhold, T., Kroon, D., Leng, M. J., Bailey, I., Röhl, U., and Zachos, J. C.: A high-fidelity benthic stable isotope record of Late Cretaceous–Early Eocene climate change and carbon-cycling, *Paleoceanography and Paleoclimatology*, 34, 672–691, 2019.
- Batenburg, S. J., Sprovieri, M., Gale, A. S., Hilgen, F. J., Hüsing, S., Laskar, J., Liebrand, D., Lirer, F., Orue-Etxebarria, X., and Pelosi, N.: Cyclostratigraphy and astronomical tuning of the Late Maastrichtian at Zumaia (Basque country, Northern Spain), *Earth Planet. Sc. Lett.*, 359, 264–278, 2012.
- Batenburg, S. J., Gale, A. S., Sprovieri, M., Hilgen, F. J., Thibault, N., Boussaha, M., and Orue-Etxebarria, X.: An astronomical time scale for the Maastrichtian based on the Zumaia and Sopolana sections (Basque country, northern Spain), *J. Geol. Soc.*, 171, 165–180, 2014.
- Beaufort, L., Bolton, C. T., Sarr, A.-C., Suchéras-Marx, B., Rosenthal, Y., Donnadieu, Y., Barbarin, N., Bova, S., Cornuault, P., Gally, Y., Gray, E., Mazur, J.-C., and Tetard, M.: Cyclic evolution of phytoplankton forced by changes in tropical seasonality, *Nature*, 601, 79–84, <https://doi.org/10.1038/s41586-021-04195-7>, 2022.
- Bralower, T., Premoli Silva, I., and Malone, M.: Leg 198, *Proceedings of the Ocean Drilling Program: Initial Reports*, College Station, TX (Ocean Drilling Program), <https://doi.org/10.2973/odp.proc.ir.198.2002>, 2002.

- Chenet, A.-L., Quidelleur, X., Fluteau, F., Courtillot, V., and Bajpai, S.: ^{40}K - ^{40}Ar dating of the Main Deccan large igneous province: Further evidence of KTB age and short duration, *Earth Planet. Sc. Lett.*, 263, 1–15, 2007.
- Clement, A. C., Seager, R., and Cane, M. A.: Orbital controls on the El Niño/Southern Oscillation and the tropical climate, *Paleoceanography*, 14, 441–456, <https://doi.org/10.1029/1999PA900013>, 1999.
- Clement, A. C., Seager, R., and Cane, M. A.: Suppression of El Niño during the mid-Holocene by changes in the Earth's orbit, *Paleoceanography*, 15, 731–737, <https://doi.org/10.1029/1999PA000466>, 2000.
- Clement, A. C., Hall, A., and Broccoli, A. J.: The importance of precessional signals in the tropical climate, *Clim. Dynam.*, 22, 327–341, <https://doi.org/10.1007/s00382-003-0375-8>, 2004.
- Crowley, T. J., Kim, K.-Y., Mengel, J. G., and Short, D. A.: Modeling 100,000-Year Climate Fluctuations in Pre-Pleistocene Time Series, *Science*, 255, 705–707, 1992.
- Dameron, S. N., Leckie, R. M., Clark, K., MacLeod, K. G., Thomas, D. J., and Lees, J. A.: Extinction, dissolution, and possible ocean acidification prior to the Cretaceous/Paleogene (K/Pg) boundary in the tropical Pacific, *Palaeogeogr. Palaeocl.*, 485, 433–454, 2017.
- Davies, A., Kemp, A. E. S., Weedon, G. P., and Barron, J. A.: El Niño–Southern Oscillation variability from the Late Cretaceous Marca Shale of California, *Geology*, 40, 15–18, <https://doi.org/10.1130/G32329.1>, 2012.
- Dymond, J., Suess, E., and Lyle, M.: Barium in deep-sea sediment: A geochemical proxy for paleoproductivity, *Paleoceanography*, 7, 163–181, 1992.
- Eagle, M., Paytan, A., Arrigo, K. R., van Dijken, G., and Murray, R. W.: A comparison between excess barium and barite as indicators of carbon export, *Paleoceanography*, 18, 1021, <https://doi.org/10.1029/2002PA000793>, 2003.
- Fedorov, A. V., Dekens, P. S., McCarthy, M., Ravelo, A. C., deMenocal, P. B., Barreiro, M., Pacanowski, R. C., and Philander, S. G.: The Pliocene Paradox (Mechanisms for a Permanent El Niño), *Science*, 312, 1485–1489, <https://doi.org/10.1126/science.1122666>, 2006.
- Forster, A., Schouten, S., Baas, M., and Sinninghe Damsté, J. S.: Mid-Cretaceous (Albian–Santonian) sea surface temperature record of the tropical Atlantic Ocean, *Geology*, 35, 919–922, 2007.
- Frank, T. D., Thomas, D. J., Leckie, R. M., Arthur, M. A., Bown, P. R., Jones, K., and Lees, J. A.: The Maastrichtian record from Shatsky Rise (northwest Pacific): A tropical perspective on global ecological and oceanographic changes, *Paleoceanography*, 20, PA1008, <https://doi.org/10.1029/2004PA001052>, 2005.
- Friedrich, O., Norris, R. D., and Erbacher, J.: Evolution of middle to Late Cretaceous oceans – A 55 m.y. record of Earth's temperature and carbon cycle, *Geology*, 40, 107–110, <https://doi.org/10.1130/g32701.1>, 2012.
- Gilbert, V., Arz, J. A., Arenillas, I., Robinson, S. A., and Ferrer, D.: Influence of the Latest Maastrichtian Warming Event on planktic foraminiferal assemblages and ocean carbonate saturation at Caravaca, Spain, *Cretaceous Res.*, 125, 104844, <https://doi.org/10.1016/j.cretres.2021.104844>, 2021.
- Gonneea, M. E. and Paytan, A.: Phase associations of barium in marine sediments, *Mar. Chem.*, 100, 124–135, 2006.
- Griffith, E. M., Thomas, E., Lewis, A. R., Penman, D. E., Westerhold, T., and Winguth, A. M.: Benthic–Pelagic Decoupling: The Marine Biological Carbon Pump During Eocene Hyperthermals, *Paleoceanography and Paleoclimatology*, 36, e2020PA004053, <https://doi.org/10.1029/2020PA004053>, 2021.
- Grinsted, A., Moore, J. C., and Jevrejeva, S.: Application of the cross wavelet transform and wavelet coherence to geophysical time series, *Nonlin. Processes Geophys.*, 11, 561–566, <https://doi.org/10.5194/npg-11-561-2004>, 2004.
- Haynes, S. J., MacLeod, K. G., Ladant, J.-B., Guchte, A. V., Ros-tami, M. A., Poulsen, C. J., and Martin, E. E.: Constraining sources and relative flow rates of bottom waters in the Late Cretaceous Pacific Ocean, *Geology*, 48, 509–513, 2020.
- Herbert, T. D. and D'Hondt, S. L.: Precessional climate cyclicity in Late Cretaceous – Early Tertiary marine sediments: a high resolution chronometer of Cretaceous–Tertiary boundary events, *Earth Planet. Sc. Lett.*, 99, 263–275, [https://doi.org/10.1016/0012-821X\(90\)90115-E](https://doi.org/10.1016/0012-821X(90)90115-E), 1990.
- Herbert, T. D., Gee, J., and DiDonna, S.: Precessional cycles in the Upper Cretaceous pelagic sediments of the South Atlantic: Long-term patterns from high-frequency climate variations, *Geological Society of America, Special Papers*, 105–120, 1999.
- Huber, B. T., MacLeod, K. G., Watkins, D. K., and Coffin, M. F.: The rise and fall of the Cretaceous Hot Greenhouse climate, *Global Planet. Change*, 167, 1–23, 2018.
- Jenkyns, H., Gale, A., and Corfield, R.: Carbon-and oxygen-isotope stratigraphy of the English Chalk and Italian Scaglia and its palaeoclimatic significance, *Geol. Mag.*, 131, 1–34, <https://doi.org/10.1017/S0016756800010451>, 1994.
- Jorissen, F. J., Fontanier, C., and Thomas, E.: Chapter Seven Paleooceanographical Proxies Based on Deep-Sea Benthic Foraminiferal Assemblage Characteristics, *Developments in Marine Geology*, 1, 263–325, [https://doi.org/10.1016/S1572-5480\(07\)01012-3](https://doi.org/10.1016/S1572-5480(07)01012-3), 2007.
- Jung, C., Voigt, S., and Friedrich, O.: High-resolution carbon-isotope stratigraphy across the Campanian–Maastrichtian boundary at Shatsky Rise (tropical Pacific), *Cretaceous Res.*, 37, 177–185, 2012.
- Jung, C., Voigt, S., Friedrich, O., Koch, M. C., and Frank, M.: Campanian–Maastrichtian ocean circulation in the tropical Pacific, *Paleoceanogr. Paleocl.*, 28, 562–573, 2013.
- Keller, G., Punekar, J., and Mateo, P.: Upheavals during the Late Maastrichtian: Volcanism, climate and faunal events preceding the end-Cretaceous mass extinction, *Palaeogeogr. Palaeocl.*, 441, 137–151, 2016.
- Kim, H. J., Kim, T., Hyeong, K., Yeh, S., Park, J., Yoo, C. M., and Hwang, J.: Suppressed CO₂ outgassing by an enhanced biological pump in the Eastern Tropical Pacific, *J. Geophys. Res.-Oceans*, 124, 7962–7973, 2019.
- Kim, J.-E., Westerhold, T., Griffith, E. M., Alegret, L., Drury, A., and Röhl, U.: Maastrichtian composite bulk carbonate stable isotopes, XRF scanning, biogenic barium, and benthic foraminiferal records from Shatsky Rise, ODP Sites 1209 and 1210, PAN-GAEA [data set], <https://doi.org/10.1594/PANGAEA.951175>, 2022.
- Laepple, T. and Lohmann, G.: Seasonal cycle as template for climate variability on astronomical timescales, *Paleoceanography*, 24, PA4201, <https://doi.org/10.1029/2008PA001674>, 2009.

- Larson, R., Steiner, M., Erba, E., and Lancelot, Y.: Paleolatitudes and tectonic reconstructions of the oldest portion of the Pacific plate: A comparative study, edited by: Larson, R. L., Lancelot, Y., Fisher, A., and Winterer, E. L., Proceedings of the Ocean Drilling Program, Scientific Results, Leg 129, 615–631, 1992.
- Laskar, J.: Chapter 4 – Astrochronology, in: Geologic Time Scale 2020, edited by: Gradstein, F. M., Ogg, J. G., Schmitz, M. D., and Ogg, G. M., Elsevier, 139–158, <https://doi.org/10.1016/B978-0-12-824360-2.00004-8>, 2020.
- Laskar, J., Robutel, P., Joutel, F., Gastineau, M., Correia, A., and Levrard, B.: A long-term numerical solution for the insolation quantities of the Earth, *Astron. Astrophys.*, 428, 261–285, 2004.
- Laskar, J., Fienga, A., Gastineau, M., and Manche, H.: La2010: a new orbital solution for the long-term motion of the Earth, *Astron. Astrophys.*, 532, A89, <https://doi.org/10.1051/0004-6361/201116836>, 2011.
- Li, L. and Keller, G.: Abrupt deep-sea warming at the end of the Cretaceous, *Geology*, 26, 995–998, 1998.
- Li, M., Hinnov, L. A., and Kump, L.: *Acycle*: Time-series analysis software for paleoclimate research and education, *Comput. Geosci.*, 127, 12–21, 2019.
- Lu, Z., Liu, Z., Chen, G., and Guan, J.: Prominent precession band variance in ENSO intensity over the last 300,000 years, *Geophys. Res. Lett.*, 46, 9786–9795, <https://doi.org/10.1029/2019GL083410>, 2019.
- Lyle, M., Dadey, K. A., and Farrell, J. W.: The Late Miocene (11–8 Ma) eastern Pacific carbonate crash: evidence for reorganization of deep-water circulation by the closure of the Panama Gateway, 1995 Proceedings of the Ocean Drilling Program, Scientific Results, 138, 821–837, 1995.
- MacLeod, K. G. and Huber, B. T.: Reorganization of deep ocean circulation accompanying a Late Cretaceous extinction event, *Nature*, 380, 422–425, 1996.
- MacLeod, K. G., Huber, B. T., Pletsch, T., Röhl, U., and Kucera, M.: Maastrichtian foraminiferal and paleoceanographic changes on Milankovitch timescales, *Paleoceanography*, 16, 133–154, 2001.
- Murray, J. W., Young, J., Newton, J., Dunne, J., Chapin, T., Paul, B., and McCarthy, J. J.: Export flux of particulate organic carbon from the central equatorial Pacific determined using a combined drifting trap-²³⁴Th approach, *Deep-Sea Res. Pt. II*, 43, 1095–1132, 1996.
- Murray, R. W., Knowlton, C., Leinen, M., Mix, A. C., and Polsky, C.: Export production and carbonate dissolution in the central equatorial Pacific Ocean over the past 1 Myr, *Paleoceanography*, 15, 570–592, 2000.
- Olivarez Lyle, A. and Lyle, M. W.: Missing organic carbon in Eocene marine sediments: Is metabolism the biological feedback that maintains end-member climates?, *Paleoceanography*, 21, PA2007, <https://doi.org/10.1029/2005PA001230>, 2006.
- Pälike, H., Norris, R. D., Herrle, J. O., Wilson, P. A., Coxall, H. K., Lear, C. H., Shackleton, N. J., Tripathi, A. K., and Wade, B. S.: The heartbeat of the Oligocene climate system, *Science*, 314, 1894–1898, <https://doi.org/10.1126/science.1133822>, 2006.
- PANGAEA: Data Publisher for Earth & Environmental Science, <https://www.pangaea.de/>, last access: 30 November 2022.
- Paytan, A., Kastner, M., and Chavez, F.: Glacial to interglacial fluctuations in productivity in the equatorial Pacific as indicated by marine barite, *Science*, 274, 1355–1357, 1996.
- Pena, L. D., Cacho, I., Ferretti, P., and Hall, M. A.: El Niño–Southern Oscillation–like variability during glacial terminations and interlatitudinal teleconnections, *Paleoceanography*, 23, PA3101, <https://doi.org/10.1029/2008PA001620>, 2008.
- Reitz, A., Pfeifer, K., De Lange, G., and Klump, J.: Biogenic barium and the detrital Ba/Al ratio: a comparison of their direct and indirect determination, *Mar. Geol.*, 204, 289–300, 2004.
- Renne, P. R., Deino, A. L., Hilgen, F. J., Kuiper, K. F., Mark, D. F., Mitchell, W. S., Morgan, L. E., Mundil, R., and Smit, J.: Time scales of critical events around the Cretaceous–Paleogene boundary, *Science*, 339, 684–687, 2013.
- Sager, W. W., Kim, J., Klaus, A., Nakanishi, M., and Khankishieva, L. M.: Bathymetry of Shatsky Rise, northwest Pacific Ocean: Implications for ocean plateau development at a triple junction, *J. Geophys. Res.-Sol. Ea.*, 104, 7557–7576, 1999.
- Scotese, C. R. and Wright, N.: PALEOMAP Paleodigital Elevation Models (PaleoDEMS) for the Phanerozoic, https://www.earthbyte.org/webdav/ftp/Data_Collections/Scotese_Wright_2018_PaleoDEM/Scotese_Wright2018_PALEOMAP_PaleoDEMs.pdf (last access: 30 November 2022), 2018.
- Scudder, R. P., Murray, R. W., Schindlbeck, J. C., Kutterolf, S., Hauff, F., and McKinley, C. C.: Regional-scale input of dispersed and discrete volcanic ash to the Izu-Bonin and Mariana subduction zones, *Geochem. Geophys. Geos.*, 15, 4369–4379, 2014.
- Short, D. A., Mengel, J. G., Crowley, T. J., Hyde, W. T., and North, G. R.: Filtering of Milankovitch cycles by Earth’s geography, *Quaternary Res.*, 35, 157–173, 1991.
- Torrence, C. and Compo, G. P.: A Practical Guide to Wavelet Analysis, *B. Am. Meteorol. Soc.*, 79, 61–78, 1998.
- Trenberth, K. E., Stepaniak, D. P., and Caron, J. M.: The global monsoon as seen through the divergent atmospheric circulation, *J. Climate*, 13, 3969–3993, 2000.
- Turk, D., McPhaden, M. J., Busalacchi, A. J., and Lewis, M. R.: Remotely sensed biological production in the Equatorial Pacific, *Science*, 293, 471–474, 2001.
- Voigt, S., Gale, A. S., Jung, C., and Jenkyns, H. C.: Global correlation of Upper Campanian – Maastrichtian successions using carbon-isotope stratigraphy: development of a new Maastrichtian timescale, *Newsl. Stratigr.*, 45, 25–53, 2012.
- Wara, M. W., Ravelo, A. C., and Delaney, M. L.: Permanent El Niño-like conditions during the Pliocene warm period, *Science*, 309, 758–761, 2005.
- Westerhold, T., Marwan, N., Drury, A. J., Liebrand, D., Agnini, C., Anagnostou, E., Barnet, J. S., Bohaty, S. M., De Vleeschouwer, D., and Florindo, F.: An astronomically dated record of Earth’s climate and its predictability over the last 66 million years, *Science*, 369, 1383–1387, 2020.
- Zachos, J., Pagani, M., Sloan, L., Thomas, E., and Billups, K.: Trends, rhythms, and aberrations in global climate 65 Ma to present, *Science*, 292, 686–693, 2001.
- Zeebe, R. E., Westerhold, T., Littler, K., and Zachos, J. C.: Orbital forcing of the Paleocene and Eocene carbon cycle, *Paleoceanography*, 32, 440–465, 2017.
- Zhang, S., Yu, Z., Gong, X., Wang, Y., Chang, F., Lohmann, G., Qi, Y., and Li, T.: Precession cycles of the El Niño/Southern oscillation-like system controlled by Pacific upper-ocean stratification, *Communications Earth & Environment*, 2, 239, <https://doi.org/10.1038/s43247-021-00305-5>, 2021.